Escola de Primavera de Transição e Turbulência Blumenau 2022
ABCM
13th Spring School on Transition and Turbulence
September 19th-23rd, 2022, Blumenau, SC, Brazil

Turbulent kinetic energy budget of a density current

Sara Mata
Jorge Silvestrini
Pontifical Catholic Rio Grande do Sul University
sara.sosa85@edu.pucrs.br
jorgehs@pucrs.br

Abstract. *Density hyperpycnal currents are flows of a denser fluid running below a lighter fluid due to density gradient. A mixing zone is developed in the fluid interface, where complex structures are generated by shear, buoyancy, and turbulence interaction, triggering processes like entrainment and mixing. At large Reynolds number (Re), density currents are fully turbulent. It is possible to delimit the mixing layer based on vorticity criterion, which identifies the layer position where the spanwise vorticity ω_z, is positive. The inner border is the vertical position where ω_z changes sign, and the diffuse outer border is chosen where ω_z achieves 5$\%$ of the maximum vorticity. This study simulated conservative density currents in lock-release configuration for Re=3450 and 8950, using Direct Numerical Simulation and Implicit Large Eddy Simulation, respectively. It is used the high-order flow solver Xcompact3d to solve a Boussinesq system on a Cartesian mesh. The statistical approach is applied to calculate fluctuations velocity via Reynolds decomposition for slumping, inertial and viscous phases. It delimited the mixing layer to compare with the turbulent kinetic energy peaks and shear production, dissipation, and buoyancy values for all the simulation times. The influence of the Re number on the evolution of the mixing layer turbulent structures are analyzed.*

Keywords: *Lock-Release configuration, turbulent kinetic energy, mixing layer, turbulence.*

1. INTRODUCTION

Density currents are flows driven by buoyancy forces induced by the specific mass difference between the current and the environment. Current propagation is determined by its ability to self-sustain these buoyant forces by limiting its dilution with the ambient fluid.

Based on experiments on gravitational density currents, Middleton (1966) divided a typical density current into three parts: head, body, and tail. In the head, the salient region, called the nose, is the result of the non-slip condition at the lower limit, an unstable density profile and friction resistance at the upper limit, causing reverse circulation and the formation of lobes and cleft structures (Kneller and Buckee, 2000). The mixing of the density current with the ambient fluid is an important process, mainly produced by entrainment. Garcia and Parson (1996) experimentally demonstrated that mixing at the head of the density stream depends on the Reynolds number Re. Density currents with high Re number are totally turbulent, with Kelvin-Helmholtz vortices at the upper part of the current. At low Re, drag is less significant, making viscous effects more important.

Although the experimental observations reveal complex velocity and density fields, the analytical modeling proposed from simplified theoretical models and numerical simulations of the Navier-Stokes equations and mass transport equation allows comparison with experimental data with acceptable accuracy.

The spreading rate of a density current could be described by the time evolution of the front velocity (Kàrmán (1940), Benjamin (1968), Shin *et al.* (2004)). Huppert and Simpson (1980) characterize the propagation of a density front in three regimes: an initial slumping phase where the current moves at an almost constant velocity, followed by an inertial phase in which the current moves under the equilibrium of buoyancy and inertial forces, and finally, a viscous phase where viscous effects dominate and balance the buoyancy. Power law expressions were obtained for the evolution of the density current front in the different phases (Hoult (1972), Huppert and Simpson (1980), Cantero *et al.* (2007b)). The turbulence structures evolution in a density current for moderate and high Re number show that the current develops the head, body, and tail at slumping phase. At the interface, strong vortex shedding continues during this phase. During the inertial phase, vortex shedding decreases in amplitude until it becomes negligible during the viscous phase (Cantero *et al.*, 2008b).

One way to understand the influence of the turbulent dynamics on the vertical profiles of velocity and density is to compute the turbulence kinetic energy (k_t) budget. At the maximum velocity, the shear production of k_t vanishes, but k_t itself does not due to advection and diffusion to the maximum velocity from the upper and lower shear layer (Dorrel *et al.*, 2019).

Ottolengui *et al.* (2017a) show the different regions of the current involved in the k_t budget. The high values of k_t are present in the current and ambient fluid interface during the slumping phase, corresponding with the Kelvin–Helmholtz vortices. The k_t budget in the mixing layer is affected by the head dilution and the subsequent loss of the buoyancy force driving the propagation of the current. The structural evolution of the current is related to the dynamics and stability of the mixing layer (Pelmard *et al.*, 2020).

This work aims to describe the time evolution of k_t budget terms to have an inside into the density current evolution dynamics.

1.1 Mathematical and Numeric Model

The incompressible Navier–Stokes equations under the Boussinesq assumption are used in the present study to describe the dynamics of the conservative density current in the lock-release configuration. For the initial time, the highest density fluid (ρ_1) is confined to the domain $L_{xb} \times L_y \times L_z$, separated by a lock from the lower density fluid (ρ_0) (Figure 1).

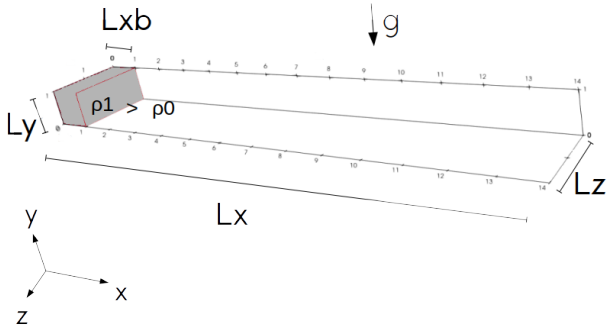

Figure 1: Initial problem setup.

The dimensionless governing equations in the Boussinesq approximation for a conservative current have the form:

$$\frac{\partial u_i}{\partial x_i} = 0 \tag{1}$$

$$\frac{\partial u_i}{\partial t} + u_j \frac{\partial u_i}{\partial x_j} = -\frac{\partial P}{\partial x_i} + \frac{1}{Re}\frac{\partial^2 u_i}{\partial x_j \partial x_j} - \varphi \delta_{i2} \tag{2}$$

$$\frac{\partial \varphi}{\partial t} + u_j \frac{\partial \varphi}{\partial x_j} = \frac{1}{ReSc}\frac{\partial^2 \varphi}{\partial x_j \partial x_j} \tag{3}$$

where u_i, P and φ correspond to the unknowns of the problem, being the velocity vector, pressure and scalar (density), respectively. Equations (1), (2) and (3) were dimensionalized using the characteristic velocity scale $U_b = \sqrt{Hg(\rho_1 - \rho_0)/\rho_0}$, with g being the gravitational acceleration and the characteristic length scale $H = L_y$. The quantities Re and Sc refer to the dimensionless Reynolds numbers $Re = U_b H/\nu$ and Schmitd $Sc = \nu/\kappa$, where ν is the kinematic viscosity and κ the mass diffusivity of the fluid ρ_1.

In order to numerically solve the equations (1), (2) and (3) was used the **Xcompact3D** code, based on the sixth-order compact finite difference scheme, in spatial differentiation, and it uses the third-order Adams-Bashforth scheme, in temporal integration. The pressure term is solved with the Poisson equation in spectral space using the fast Fourier transform (Bartholomew *et al.*, 2020).

The velocity field boundary conditions established on the x axis is free slip, and on the z axis it is periodicity. In the case of the y axis it is non-slip at $y = 0$ and free slip at $y = L_y$. For the scalar field, the boundary conditions for the axes x and y are zero flux, and for the axis z it is periodicity.

The Reynolds numbers considered are $Re = 3450$ and 8950. The choice of these values is based on the problem addressed in Cantero *et al.* (2007b) to make comparisons that validate the results obtained in the simulations. For these moderate values of Re, the current behavior is little sensitive to the Schmidt number (Haertel *et al.*, 2000), therefore it is considered $Sc = 1$.

The computational domain is a parallelepiped $L_x \times L_y \times L_z = (14, 1, 2)$. In this domain it is possible to visualize the evolution of the different phases of the density current. The mesh resolution used for all simulations is $N_x = 1945, N_y = 121, N_z = 240$. The $Re = 3450$ simulation is solved using Direct Numerical Simulation (DNS) approach while the $Re = 8950$ simulation with Implicit Large-Scale Simulation (iLES), based on the spectral turbulent viscosity model (Lamballais *et al.* (2011), Dairay *et al.* (2017)).

1.2 Statistical approach

The statistical treatment of turbulence is based on the Reynolds decomposition of the physical quantities, which aims to dissociate the averaged behavior of the flow from the local variations due to turbulent perturbations. Introducing the

Reynolds ensemble-averaging operator, each physical quantity u_i is decomposed as

$$u_i = \overline{u_i} + u_i', \tag{4}$$

where $\overline{u_i}$ represents the spanwise averaged value of u_i and u_i' is the turbulent velocity fluctuations about this average.

The turbulent energy budget is obtained from the mean kinetic energy of the turbulent velocity fluctuations equation,

$$k_t = \frac{1}{2}\overline{u_i' u_i'}. \tag{5}$$

Multiplying the Navier-Stokes equations (Eq. 2) by u_i', taking the time average of all terms, subtracting the energy equation for the mean flow, and integrating into the volume control V, it is found (Tennekes and Lumley, 1972),

$$\frac{d}{dt}k_t = \underbrace{\int_V -\overline{u_i' u_j'}\frac{\partial \bar{u}_i}{\partial x_j} dV}_{\mathscr{P}} + \underbrace{\int_V -\overline{u_2' \varphi'} dV}_{\mathscr{B}} - \underbrace{\int_V \frac{1}{Re}\overline{\frac{\partial u_i'}{\partial x_j}\frac{\partial u_i'}{\partial x_j}} dV}_{\varepsilon}. \tag{6}$$

The $\mathscr{P}$ term refers to the production of turbulence by shear, representing energy conversion from the mean flow to turbulent fluctuation. The $\mathscr{B}$ term is the buoyancy flux responsible for the production/destruction of turbulence (positive/negative) due to buoyant mixing in stratified flows. The ε term represents the viscous dissipation of turbulence representing energy loss.

2. RESULTS

2.1 Front Velocity

Initially, the front current velocity (V_f) is computed from the Average Thickness Layer minimum local method at the front (Farenzena and Silvestrini, 2022). Figure 2 shows the evolution of the temporal front velocity for the two Reynolds numbers (3450 and 8950) numerical simulations. It also includes the scale laws of the different propagation phases (Cantero *et al.*, 2007b) which identify the transition times between the different phases. For the higher Re number, the density current transits from the slumping phase to the inertial phase at $t \sim 12$, extending for a short period until $t \sim 18$ and then passing through the viscous phase until it dissipates. In the lower Re simulation case, the current directly transitions from the slumping phase to the viscous phase at the $t \sim 15$ without passing through the inertial phase. The simulations show a good agreement with the reference.

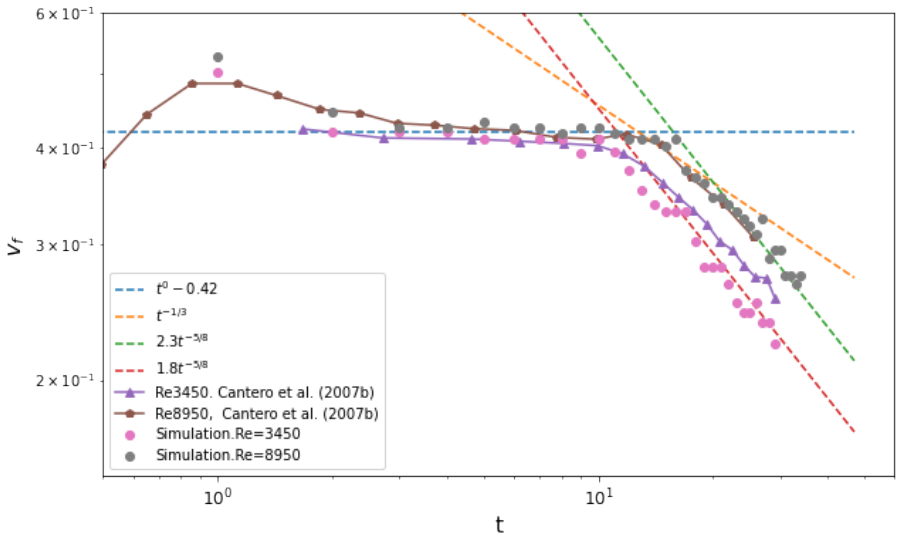

Figure 2: Time evolution of the front velocity.

2.2 Turbulent Kinetic Energy and the Mixing Layer

The mixing layer develops at the interface of two parallel fluid streams that move horizontally with different velocities and densities. It is characterized by instabilities that develop a mixing process. Density current with a high Reynolds number (Re) develops Kelvin-Helmholtz instability, forming Kelvin-Helmholtz billows (Brown and Roshko, 1974). It is

possible to identify the vortex structure from the vorticity ($\omega = \nabla \times \mathbf{u}$). Inside the current, in the near-wall zone $\omega_z < 0$ and in the mixing layer $\omega_z > 0$. Thus, the layer where ω_z change sign is considered the inner mixing layer. The diffuse outer border is defined where ω_z achieves 5% of the maximum vorticity value. For the $Re = 8950$ case at $t = 12$, this value is 0.032 and the $Re = 3450$ case at $t = 15$ the value is 0.013. The choice of these particular times is due to the maximum value of the turbulent kinetic energy (Eq.5) k_t as it is shown in Figure 3(a). For both Re cases is observed an increase of k_t, until the $t = 8$ for $Re = 8950$ case and the $t = 15$ for $Re = 3450$ case. This region is related to the constant velocity phase (slumping phase), being the k_t values for $Re = 3450$ case much smaller than the $Re = 8950$ case. Kelvin-Helmholtz vortices begin to appear in this phase, going up to $t = 15$ for the $Re = 3450$ case, when the collapse of the vortices is observed (Figure 3b). At this time, it reaches the highest value of k_t, which starts to decrease in the viscous phase, where the current dissipates. For all times, the k_t distribution shows higher values in the region of the mixing layer, characterized by the presence of intense shear. Similar results were revealed for the $Re = 8950$ case. During the slumping phase, Kelvin-Helmholtz vortices are observed, which develop until they break up at $t \sim 10$. This time coincides with the time of maximum k_t value, which remains almost constant until $t = 20$, during the inertial phase. After the collapse of the vortices, the generation of smaller-scale structures and loss of vortex coherence is observed. Finally, the turbulence dissipates in the viscous phase. These results could suggest that turbulence is more effective in the transition of slumping to the inertial phase, where the maximum value of k_t coincides with the collapse of the Kelvin-Helmholtz vortices.

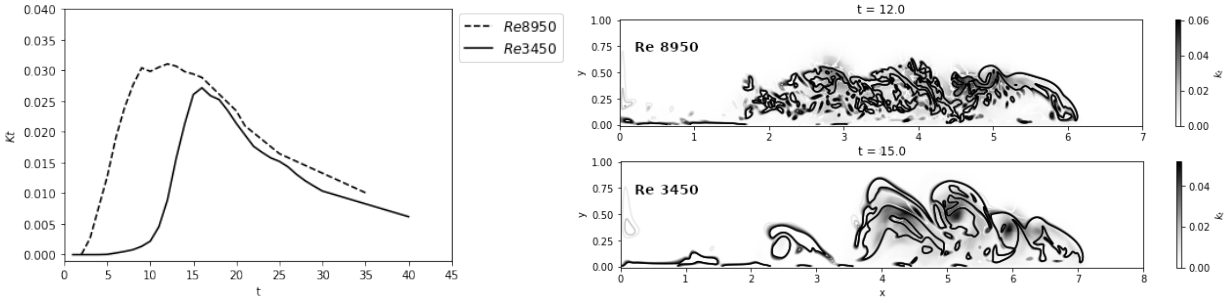

(a) Time evolution of k_t

(b) Span-averaged k_t

Figure 3: Time evolution of Turbulent Kinetic Energy (k_t) for Re 8950 and 3450 (a), Span-averaged k_t along the current at the time of maximum k_t value for $Re = 8950$ (up b) and $Re = 3450$ (down b). The contour lines correspond to the mixing layer, where $0<\omega_z<0.05\omega_{z,max}$

2.3 Turbulent Kinetic Energy Budget

The evolution of the different terms of the turbulent kinetic energy budget (Eq. 6) could give us an idea about the source/sink of turbulence in the density current spreading. Figure 4 shows the contribution k_t, $\mathscr{P}$, $\mathscr{B}$, ε, for the $Re = 8950$ case at $t = 10$. The region with higher k_t values is the mixing layer which shows the maximum in the center of roll-up Kelvin-Helmholtz vortices. The current head and nose region also presents k_t values that could be related to the lobes and cleft structures.

The production of k_t by shear stress $\mathscr{P}$, which extracts energy from the mean flow, has positive values in the Kelvin-Helmholtz vortices and near-wall regions. The current nose presents negative values, which means suppressing of k_t.

The turbulence driven by buoyancy $\mathscr{B}$ shows positive values due to unstable configurations. Positive $\mathscr{B}$ values are observed in the current head, with maximum value in the current nose. Positive and negative $\mathscr{B}$ values are present in the Kelvin-Helmholtz vortices region, with negative values in the vortex center.

The viscous dissipation ε is present in the current and ambient interface: the Kelvin-Helmholtz vortices region, the current head, and the bottom. The Kelvin-Helmholtz vortices region presents the higher dissipation.

The time evolution of the turbulent kinetic energy budget terms (Figure 5) exhibits a dynamic of the density current spreading for moderate Reynolds number. At initial times($t \sim 4$) related with slumping phase all terms increase until the $t = 10$ for $Re = 8950$ and $t = 15$ for $Re = 3450$, where they reach the maximum value. In the $Re = 3450$ case, the increase is slowly until $t = 10$. After this, it shows an abrupt increase until $t = 15$. Possibly this is the transition time to the incoming phase. The increase in all terms is related to turbulent growth, visible with the Kelvin-Helmholtz eddies. For the $Re = 8950$ case, after the $t = 10$ begins the inertial phase. The production $\mathscr{P}$ and ε terms rapidly decrease until $t = 20$. The Buoyancy $\mathscr{B}$ term shows a decrease to negative value suggesting a buoyant stable configuration. It could mean that only the production of turbulence by shear contributes to the turbulent kinetic energy in the inertial phase. All turbulent kinetic energy budget terms decrease to low values in the viscous phases, for the $Re = 3450$ case, after $t = 15$, and the $Re = 8950$ case, after $t = 20$.

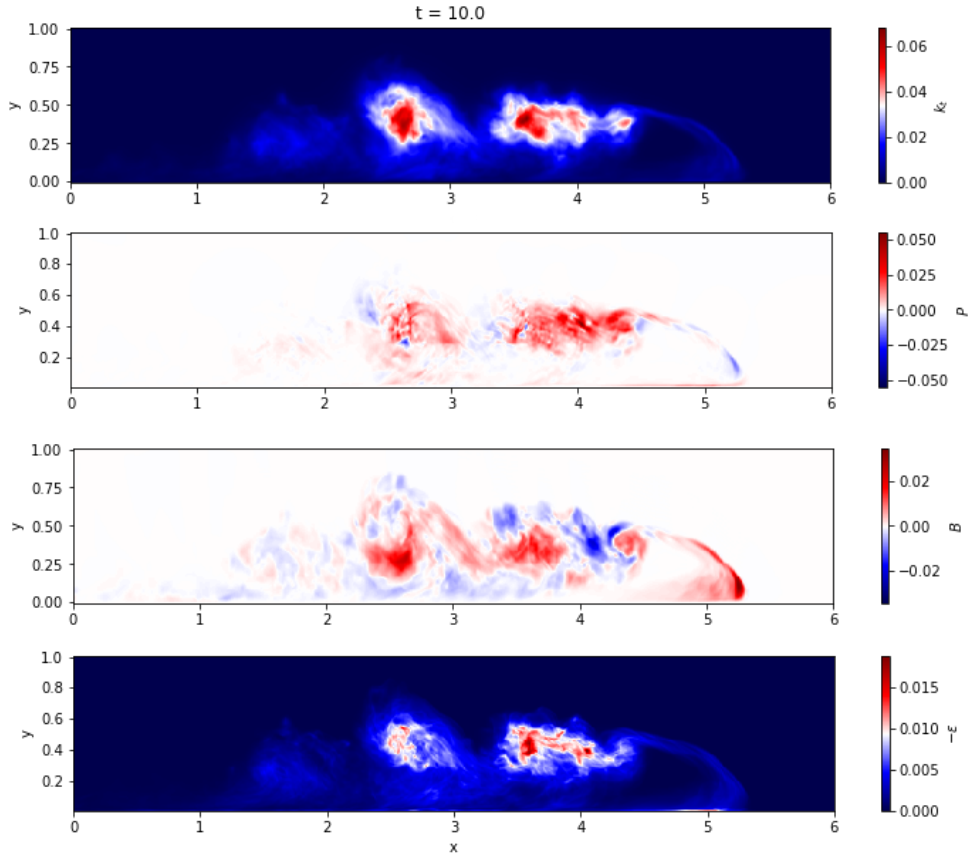

Figure 4: Turbulent kinetic energy budget terms for $Re = 8950$ at $t = 10$

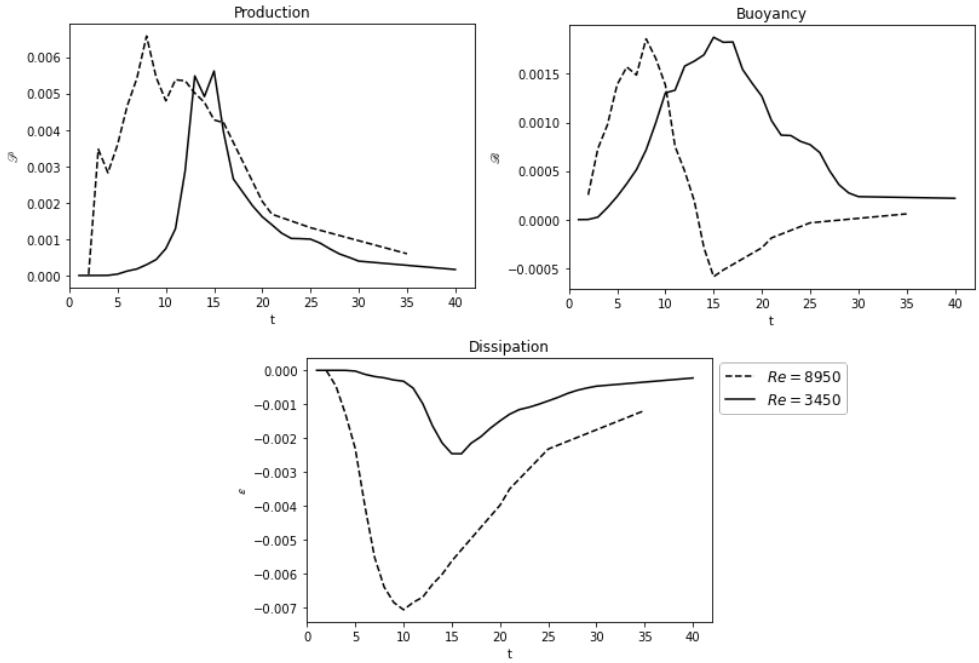

Figure 5: Time evolution of turbulent kinetic energy budget terms; Production, Buoyancy and Dissipation, for $Re = 8950$ and $Re = 3450$

3. CONCLUSION

Density currents simulations in lock-exchange configuration have been performed to evaluate the turbulent development characterized by the turbulent kinetic energy. Two moderate Reynolds numbers were considered: $Re = 3450$ and

$Re = 8950$. The lower Reynolds number was performed using the DNS approach, while the higher Reynolds number with the iLES approach. Reynolds decomposition was used to separate the mean flow from the turbulent fluctuations. The rough statistics performed were computed from the span-average of momentum and scalar field to calculate the turbulent kinetic energy and the terms contributing to its budget. The mixing layer was computed from the vorticity approach, observing that the distribution of k_t shows higher values in the region characterized by shear stress. The time evolution of k_t budget allowed us to distinguish the different phases of the current spreading. The results suggest that turbulence development is higher at the end of the slumping phase. The maximum value of k_t budget terms coincides with the collapse of the Kelvin-Helmholtz vortices. It was also possible to observe in the k_t budget terms, the current regions where the turbulence is developing. The mixing layer showed the higher values of all terms related to the Kelvin-Helmholtz billows. The current head presented significant values at the nose and bottom, related to lobes and cleft structures. The turbulence driven by shear stress was most significant in the mixing layer. The turbulence driven by buoyancy showed an unstable configuration in the current head and some spots in the mixing layer. More simulations with higher Re number are necessary to better understand the inertial phase dynamics, with the Buoyancy negative values, and more simulations with lower Re number to better understand the slumping phase dynamics with the slope change in the k_t budget terms.

4. ACKNOWLEDGEMENTS

Present simulations have been carried out at the Pontifical Catholic University of Rio Grande do Sul (PUCRS) High-Performance Computing facility LAD. The authors are grateful for the financial assistance of CAPES.

5. REFERENCES

Bartholomew, P., Deskos, G., Frantz, R., Schuch, F., Lamballais, E. and Laizet, S., 2020. "An open-source framework for solving turbulence problems on a cartesian mesh". *SoftwareX*, Vol. 12, p. 100550.

Benjamin, T., 1968. "Gravity currents and related phenomena". *J. Fluid Mech.*, Vol. 31, p. 209–248.

Brown, G. and Roshko, A., 1974. "On density effects and large structure in turbulent mixing layers". *J. Fluid Mech*, Vol. 64, pp. 775–816.

Cantero, M., Balanchandar, S., Garcia, M. and Bock, D., 2008b. "Turbulent structures in planar gravity currents and their influence on the flow dynamics". *J. Geophys. Res*, Vol. C08018, p. 113.

Cantero, M., Lee, J., Balanchandar, S., Garcia, M. and Bock, D., 2007b. "On the front velocity of gravity currents". *J. Fluid Mech*, Vol. 586, pp. 1–39.

Dairay, T., Lamballais, E., Laizet, S. and Vassilicos, J., 2017. "Numerical dissipation vs. subgrid-scale modelling for large eddy simulation". *Journal of Computational Physics*, Vol. 337, pp. 252–274. ISSN 0021-9991. doi: https://doi.org/10.1016/j.jcp.2017.02.035.

Dorrel, R., Peakall, J., Darby, S., Parsons, D., Johnson, J., Sumner, E., Wynn, R., Özsoy, E. and Tezcan, D., 2019. "Self-sharpening induces jet-like structure in seafloor gravity currents". *Nat. Commun.*, pp. 1–10.

Farenzena, B. and Silvestrini, J., 2022. "Density currents front velocity uncertainty". *Computers and Fluids*, Vol. 232.

Garcia, M. and Parson, J., 1996. "Mixing at the front of gravity currents". *Dyn. Atmos. Oceans*, Vol. 24, p. 197–205.

Haertel, C., Meiburg, E. and Necker, F., 2000. "Analysis and direct numerical simulation of the flow at a gravity-current head. part 1. flow topology and front speed for slip and no-slip boundaries". *J. Fluid Mech.*, Vol. 418, pp. 189 – 212.

Hoult, D., 1972. "Oil spreading in the sea". *Annu. Rev. Fluid Mech.*, Vol. 4, p. 341–368.

Huppert, H. and Simpson, J., 1980. "The slumping of gravity currents". *J. Fluid Mech.*, Vol. 99, pp. 785–799.

Kneller, B. and Buckee, C., 2000. "The structure and fluid mechanics of turbidity currents: a review of some recent studies and their geological implications". *Sedimentology*, Vol. 47, p. 62–94.

Kàrmán, T.V., 1940. "The engineer grapples with nonlinear problems". *Bull. Am. Math. Soc.*, Vol. 46, p. 615–683.

Lamballais, E., Fortuné, V. and Laizet, S., 2011. "Straightforward high-order numerical dissipation via the viscous term for direct and large eddy simulation". *Journal of Computational Physics*, Vol. 230, pp. 3270–3275.

Middleton, G., 1966. "Experiments on density and turbidity currents, i. motion of the head". *Can. J. Earth Sci*, Vol. 3, p. 523–46.

Ottolengui, L., Adduce, C., Roman, E. and Armenio, V., 2017a. "Analysis of the flow in gravity currents propagating up a slope". *Ocean Model*, Vol. 115, pp. 1–13.

Pelmard, J., Norris, S. and Friedrich, H., 2020. "Statistical characterization of turbulence for an unsteady gravity current". *J. Fluid Mech.*, Vol. A7. doi:https://doi.org/10.1017/jfm.2020.528.

Shin, J., Dalziel, S. and Linden, P., 2004. "Gravity currents produced by lock exchange". *Journal of Fluid Mechanics*, Vol. 521, p. 1–34. doi:10.1017/S002211200400165X.

Tennekes, H. and Lumley, J., 1972. *A First Course in Turbulence*. MIT Press, Massachusetts.

6. RESPONSIBILITY NOTICE

The authors are the only responsible for the printed material included in this paper.